Food Packaging and Shelf Life 31 (2022) 100807

Contents lists available at ScienceDirect

Food Packaging and Shelf Life

journal homepage: www.elsevier.com/locate/fpsl

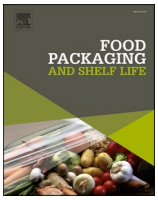

Development of sustainable food packaging material based on biodegradable polymer reinforced with cellulose nanocrystals

Marcio S. Andrade [a], Otávio H. Ishikawa [a], Robson S. Costa [a], Marcus V.S. Seixas [a], Rita C.L. B. Rodrigues [b], Esperidiana A.B. Moura [a,*]

[a] Instituto de Pesquisas Energéticas e Nucleares, Centro de Química e Meio Ambiente, 2242 Prof. L. Prestes Av., 05508-000 São Paulo, SP, Brazil
[b] Universidade de São Paulo, Escola de Engenharia de Lorena, 12602-810 Lorena, SP, Brazil

ARTICLE INFO

Keywords:
Cellulose nanocrystals
Sustainable packaging
Bionanocomposite film
Agro-waste
Sugarcane bagasse
Biomass pretreatment

ABSTRACT

The increased environmental impact and sustainability issues related to conventional food packaging have gained attention and led to a global concern. The massive consumption of conventional food packaging has increased disposal of non-eco-friendly packaging waste, severely damaging the environment. The replacement by sustainable packaging is an important alternative to reduce the enormous volume of plastic waste. In this work, bionanocomposite films composed of PBAT/PLA blend and cellulose nanocrystals (CNCs) extracted from agro-waste were investigated. Characterization of CNCs confirmed that nanocrystals were obtained. Bionanocomposite films presented better hydrophobic character and thermal stability than the blend film. In addition, the tensile strength, elongation at break, and Young's modulus was around 52%, 29%, and 118%, respectively, higher than blend films. These mechanical values were comparable to values of commercial plastic materials that are extensively used in food packaging. Thus, the prepared bionanocomposite films might be an interesting alternative to produce sustainable food packaging materials.

1. Introduction

Packaging materials based on conventional plastic petroleum-derived polymers are traditionally used in the food packaging industry. A variety of practically non-degradable and not recyclable petroleum-derived plastic, metal, glass, paper, and board, in various combinations, are also employed to achieve the properties for essential functions of food packaging that maintain the quality and safety of food (Coles & Kirwan, 2003; Marsh & Bugusu, 2007). Although their exceptional properties, such as lightweight, water resistance, barrier against the transfer of liquids and gases, good mechanical behavior, and heat sealability maintain the safety and quality of food products from processing and manufacturing to consumer use, the practically non-degradability, not recyclability, and other negative impacts at the end of their short shelf life have increased the global environmental awareness and driven attention to developing alternative raw materials from renewable resources (Coles & Kirwan, 2003; Marsh & Bugusu, 2007; Raheem, 2013). Although the packaging is indispensable for maintaining the quality and freshness of food and extending its lifetime, the increased production and consumption of conventional food packaging have increased non-eco-friendly packaging waste disposal, severely damaging the eco and aqua systems and, consequently, human and animal health. Thus, the replacement of conventional packaging for sustainable alternatives that easily and safely degrade is a vital alternative to decrease disposal of plastic wastes in landfills, rivers, and marine environments (Gan & Chow, 2018; Raheem, 2013; Zhong, Godwin, Jin, & Xiao, 2020).

Some commercially available biopolymers are attractive alternatives to prepare sustainable food packaging materials. Among the commercial biopolymers, poly(lactic acid) (PLA) is a polyester polymer with high modulus and strength comparable to that of petroleum-derived plastics, and poly(butylene adipate-co-terephthalate) (PBAT), an aliphatic-aromatic copolyester, is a highly flexible biopolymer whose properties are comparable to those of low-density PE (LDPE).

The blend of PLA and PBAT has drawn much attention as a promising material for sustainable food packaging (Gan & Chow, 2018; Moustafa, Youssef, Darwish, & Abou-Kandil, 2019; Vasile, 2018; Zhong et al., 2020). The high toughness of PBAT makes it the right candidate, and it is industrially viable for blending with PLA to develop a more appropriate bionanocomposite for the sustainable packaging field. The high

* Corresponding author.
E-mail address: eabmoura@ipen.br (E.A.B. Moura).

https://doi.org/10.1016/j.fpsl.2021.100807
Received 13 April 2021; Received in revised form 27 November 2021; Accepted 30 December 2021
Available online 10 January 2022

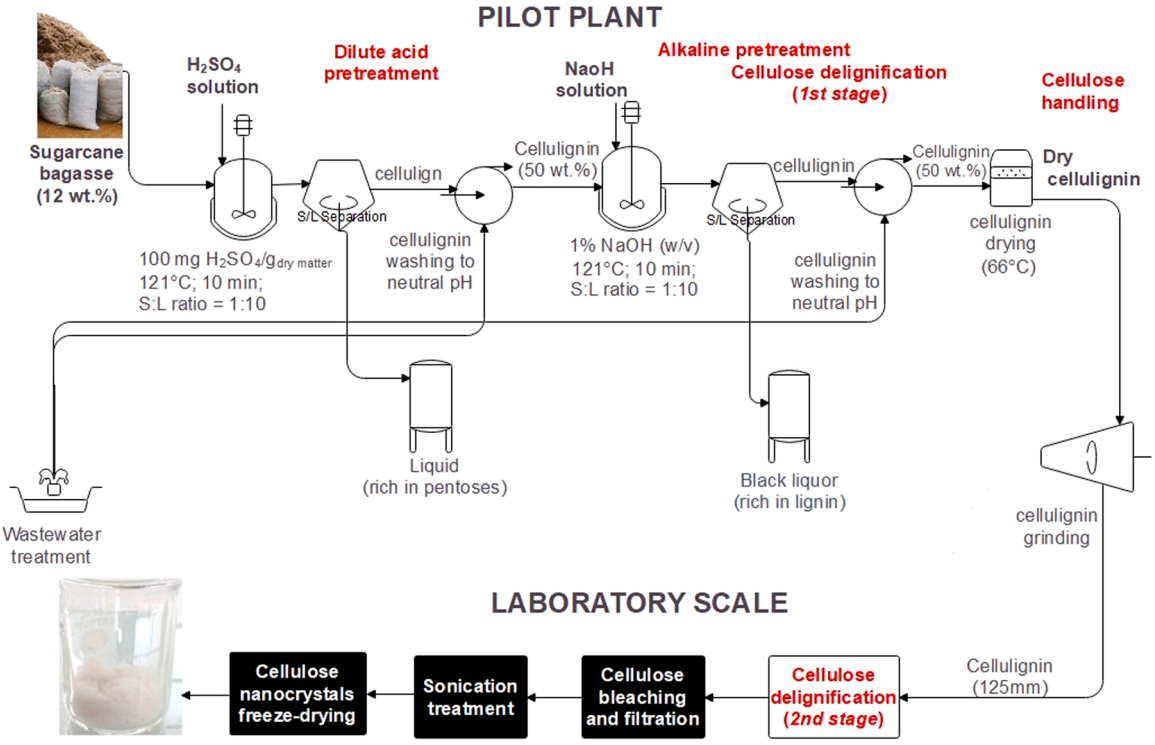

Fig. 1. Schematic representation for synthesis of CNCs.

toughness of PBAT makes it the right candidate, and it is industrially viable for blending with PLA to develop a more appropriate bionanocomposite for the sustainable packaging field. Blends of PLA and PBAT are an excellent alternative to combine properties of both polymers; however, they tend to result in immiscible blends, as their physical properties are highly dependent on their morphological characteristics. However, miscible or compatible systems are commonly observed in copolymer-homopolymer mixtures, even in the absence of specific interactions (Rana, Mandal, & Bhattacharyya, 1993; Rana, Mandal, & Bhattacharyya, 1996; Rana, Bag, Bhattacharyya, & Mandal, 2000). The compatibility between the PLA and PBAT blend can be evaluated by Fourier transform infrared (FTIR), nuclear magnetic resonance (NMR) spectroscopy, dynamic mechanical analysis, as well as observed by SEM and TEM.

Therefore, for the PLA/PBAT blends to be suitable as a competitive, sustainable food packaging material compared to traditional ones, the thermal stability, UV, water vapor, and gas barrier properties must be improved. Different techniques have been highlighted to address these limitations, such as chemical modification and reinforcing nanofillers (Kumar, Mukherjee, & Dutta, 2020; Moustafa et al., 2019; Vasile, 2018; Yadav & Chiu, 2019). The synergistic effects of fillers at the nanoscale level are because of the higher surface/volume ratio – the smaller the particle size, the larger the ratio. Their interaction with biopolymers can results in food packaging material with adequate performance and economic profitability, which can expand their commercial application (Hai, Choi, Zhai, Panicker, & Kim, 2020; Papadopoulou et al., 2019; Risyon, Othman, Basha, & Talib, 2020; Rocca-Smith et al., 2019). Several nanofiller types can be used to prepare bionanocomposite for food packaging applications, including nanocellulose. The positive aspects of nanocellulose as a sustainable nanomaterial are its abundance, renewability and biodegradability, high mechanical properties, high reinforcing capability, and low density. Two types of nanocellulose can be obtained from cellulose. One of the main constituents of plant cell walls is cellulose nanocrystals (or "nanowhiskers") (CNCs), which exhibit a needle-like appearance. The other type is nanofibrillated cellulose (CNF), which refers to long and flexible nanofillers composed of alternating amorphous and crystalline domains (Dufresne, 2018; El Fawal et al., 2020; Gan, Sam, Abdullah, & bin, Omar, 2020; Jamróz, Kulawik, & Kopel, 2019; Moustafa et al., 2019; Risyon et al., 2020; Yadav & Chiu, 2019; Zhong et al., 2020).

Thus, PBAT/PLA/CNCs films have great potential in the food packaging industry, requiring further studies in the literature. This work aims to prepare sustainable bionanocomposite films composed of a biodegradable poly(lactic acid)/poly(butylene adipate-co-terephthalate) blend containing different amounts of cellulose nanocrystals (CNCs, 0–2 wt.%), extracted from agro-waste using a twin-screw extruder and blown extrusion process. The synthesis techniques adopted in this work were innovative as the bionanocomposite was prepared by extrusion process from a biodegradable blend, in a simple, rapid, eco-friendly, and easily reproducible manner. The cellulose nanocrystals used to prepare the bionanocomposite were extracted from agro-waste and have an economic advantage because only small amounts of nanofillers are needed to increase the performance of the film. The nanocomposite film packaging was produced by blown extrusion, an industrial process. The effect of CNC content on the morphological, mechanical, and thermal properties of the films was assessed to evaluate the potential use of the bionanocomposite films for sustainable food packaging applications. These novel food packaging materials presented mechanical values comparable to those of some commercial plastic-based films used in flexible food packaging.

2. Materials and methods

2.1. Materials

Sugarcane bagasse fiber (SBF) waste were obtained from Usina Iracema, São Martinho Group in Iracemápolis, São Paulo, Brazil. The moisture content of the raw SBF fibers was around 50 wt. %. PLA Ingeo™ 2003D, from NatureWorks, PBAT (Ecoflex F C1200) from BASF. The analytical grade chemicals used in this work were purchased from Sigma-Aldrich and used without further purification.

Table 1
Chemical composition of *in natura* sugarcane bagasse fiber ($SBF_{in\ natura}$) and after diluted sulfuric acid pretreatment (SBF_{acid}), as sell as the first alkaline pretreatment (SBF_{alcali}).

Constituent	$SBF_{in\ natura}$ (mass %)	SBF_{acid} (mass%)	SBF_{alcali} (mass %)
Cellulose	45.07 ±2.08	62.57 ±3.86	85.96 ±1.51
Hemicellulose	29.78 ±1.50	0	0
Soluble Lignin	0.70 ±0.08	0.31 ±0.04	0.08 ±0.06
Insoluble Lignin	12.27 ±1.74	34.21 ±6.86	13.50 ±7.61
Extractives	3.12 ±0.27	0	0
Ash	6.02 ±0.73	6.05 ±0.93	10.81 ±1.38
Total	96.97 ±6.40	103.1 5 ±11.6	110.34 ±10.57

2.2. Isolation and Characterization of Cellulose Nanocrystals (CNCs)

2.2.1. Cellulose delignification (first stage)

The CNCs were prepared from SBF waste using the dilute sulfuric acid pretreatment process conducted in the Pilot Plant at Engineering School of Lorena - University of São Paulo (EEL-USP). First, the SBF was sun-dried until it reached a humidity of about 12 wt.%. The dilute sulfuric acid pretreatment (100 mg sulfuric acid/mg dry matter) was performed in a stainless steel AISI 316 reactor, with a total volumetric capacity of 50 liters, equipped with a jacket for indirect heating by electric resistance. The reaction was conducted at 121 °C for 10 min, the ratio of solid: liquid was 1:10 (Rodrigues et al., 2010), obtaining the SBF pretreated by diluted acid (cellulignin - SBF_{acid}). The cellulignin from sugarcane bagasse pretreated by diluted sulfuric acid was washed until neutral pH and dried to 50 wt. %. In the same pilot plant, the first stage of cellulignin delignification (Fig. 1) was performed by alkaline pretreatment using 1.0% (w/v) NaOH in the ratio of solid: liquid of 1:10 at 121 °C and reaction time of 10 min (Mori, 2015). Then, the partially delignified material (cellulignin) was separated from the soluble lignin-rich black liquor fraction by centrifugation. The cellulignin fraction was washed with water to near neutral pH, dried in the air circulating oven at 60 °C, milled in a ball mill, and classified according to particle size. Cellulose with particle size smaller than 125 μm was submitted to the second delignification process on the laboratory scale. For that, cellulose fiber was treated with 4% (w/v) NaOH solution at 70 °C and for 1 hour under constant magnetic stirring. This procedure was repeated until the NaOH solution remained colorless after extraction. The second stage of cellulose delignification was to remove the lignin residue from the cellulose. The overall synthesis process of CNC is schematically summarized in Fig. 1.

The chemical composition of *in natura* sugarcane bagasse fiber ($SBF_{in\ natura}$) and after diluted sulfuric acid pretreatment (SBF_{acid}) and first alkaline pretreatment (SBF_{alcali}) are provided in Table 1.

2.2.2. Cellulose delignification (second stage)

The cellulose fibers were bleached with 8% (w/v) NaOH solution and 24% (v/v) H_2O_2 at a ratio of 1:1 for 1 hour at 50 °C under magnetic stirring, using 1 g fiber to 10 mL solution ratio. After the bleaching step, the solution of cellulose fibers was vacuum filtered and dried in a circulating oven at 60 °C. After the bleaching step, the cellulosic material was hydrolyzed using a 65% (w/w) aqueous sulfuric acid solution, maintaining the ratio of 1 g fiber to 10 ml H_2SO_4 solution at 45 °C for 60 min under magnetic stirring. The acid hydrolysis allows a chemical attack on the amorphous regions most susceptible to reaction with sulfuric acid. In turn, after the addition of sulfuric acid, the crystalline regions of cellulose remain unchanged. The high concentration of sulfuric acid was used to guarantee the efficiency of the chemical attack on the amorphous region. After acid hydrolysis, the cellulose was subsequently dialyzed with distilled water in a cellulose membrane (Sigma-Aldrich: D9402) until the pH value between 6 and 7 to reduce the excess acidity of the solution and interrupt the chemical reaction of the cellulose fiber with sulfuric acid. Then it was frozen and freeze-dried for 24 hours to obtain the powder.

2.2.3. Sonication treatment

In this work, sonication treatment was used to obtain cellulose nanocrystal (CNC). For the sonication step, 2 g of freeze-dried cellulose fiber powder was added for every 250 ml of water/DMF (dimethylformamide)/ethanol solution in an 8:1:1 volume ratio. Sonication treatment was performed using an ultrasonic processor, model VCX 750 (Sonics & Materials, Inc), with 20 kHz ultrasonic frequency at 70%, 750 Watts. After sonication treatment, the cellulose nanocrystals were visibly dispersed (Fig. 1).

2.2.4. Freeze-drying of cellulose nanocrystals

To incorporate the cellulose nanocrystals into the PBAT/PLA blend through the extrusion process, the aqueous cellulose nanocrystal samples were frozen and freeze-dried for 24 hours in an MSSL-404 vial freeze dryer with an internal platform and microprocessor vacuum, pressure stabilized at 60 mmHg and temperature of -42 °C.

2.3. Preparation of blend and bionanocomposite films

The pellets of both PBAT and PLA were initially dried in an air circulating oven at a temperature of 60 °C for 24 hours, to remove moisture content to less than 2% before processing. Blend of PBAT/PLA (70/30 wt. %) was mixed through a dry blender operated at 80 rpm and 40 °C temperature for 10 min. The neat premixed dry blend and blend containing 1–2% (wt. %) of freeze-dried cellulose nanocrystals were melt blended in a corotating twin-screw extruder Haake Rheomex with 16 mm and L/D = 25 rate from Thermo Scientific. The temperature profile was 95/118/125/135/135/135 °C. The screw speed was 50 rpm. The extrudates coming out of the extruder were cooled down for better dimensional stability, pelletized by a pelletizer, dried again at 60 ± 2 °C for 4 hours, and fed into extrusion blown film, single-screw extruder Haake Rheomex with 16 mm and L/D = 25 rate from Thermo Scientific, and flexible film samples were obtained. The temperature profile was 120/125/130/130/135/135 °C, the blow-up ratio (BUR) of the bubble was 2:1, and screw rotation was kept at 30 rpm.

2.4. Characterization of cellulose nanocrystal

2.4.1. X-ray diffraction (XRD) analysis

The crystalline structure and crystallinity index of SBF and cellulose nanocrystal (CNC) were determined by XRD analysis. The XRD data were collected using a Rigaku multiflex diffractometer. These measurements were performed using Cu Kα (λ=1,5418 Å), under the operational conditions of 40 kV and 20 mA, over the 2θ range from 5° to 90°. The crystallinity index of the samples was calculated using Eq. (1) (Yadav & Chiu, 2019):

$$IC\ (\%) = (((I002\text{-}Iar)/I002)\ x\ 100) \quad (1)$$

Where IC is the crystallinity index; I002 is the intensity of the crystalline region of cellulose (2θ=22.5°); Iar is the intensity of the amorphous region (2θ=16.5°) (Yadav & Chiu, 2019).

2.4.2. Thermogravimetric analysis (TGA)

The thermal degradation of all cellulosic samples (SBF and CNC) was investigated using thermogravimetric analysis. Thermogravimetric analysis (Mettler-Toledo – TGA/SDTA 851) was performed under a nitrogen atmosphere (50 mL min^{-1}). The samples (approximately 10 mg) were heated from 30 to 800 °C at a heating rate of 10 °C/min. The weight loss (%) was evaluated by measuring the residual weight at 770 °C.

2.4.3. Transmission electron microscopy (TEM)

The suspensions containing 10, 30, and 50 mg/mL of cellulose nanocrystals in water were prepared for transmission electron microscopy analysis. A droplet of diluted suspension was deposited on a

copper screen covered with a carbon support film. The prepared samples were stained with a 1.5% solution of uranyl acetate, dried at room temperature, and observed by TEM using a Tecnai FEI G20 with an acceleration voltage of 200 kV. Measurements of cellulose nanocrystal dispersion in water were also taken before and after lyophilization and further dispersion by ultrasonic treatment.

2.5. Characterization of blend and bionanocomposite films

2.5.1. Thermogravimetric analysis (TGA)

Thermogravimetric analysis (Mettler-Toledo – TGA/SDTA 851) was performed under a nitrogen atmosphere (50 mL min^{-1}). The samples (approximately 10 mg) were heated from 25 to 600 °C at a heating rate of 10 °C/min. The weight loss (%) was evaluated by measuring the residual weight at 600 °C.

2.5.2. Differential Scanning Calorimetry (DSC) analysis

DSC analyses were carried out using a Mettler Toledo DSC 822e from 25 to 250 °C at a heating rate of 10 °C/min under a nitrogen atmosphere (50 ml/min). All samples were first heated from 25 to 250 °C at a rate of 10 °C/min, rapidly cooled to 25 °C, and reheated to 250 °C at 10 °C/min to provide thermal history. T_m and ΔH_m were determined considering the heat capacity change observed on the second heating. Furthermore, since the PBAT fraction is the crystalline phase of the films and PLA is an amorphous phase, the degree of crystallinity (X_c) was determined from the sample melting enthalpy considering only the PBAT fraction as being the crystalline phase of the films. The PBAT degree of crystallinity (Xc) was determined by Eq. 2 (Xiao, Lu, & Yeh, 2009):

$$X_c = \left(\Delta H_m / \Delta H_m{}^0 \quad (1\text{-}W_{PBAT}) \times 100\%\right) \tag{2}$$

Where X_c is the degree of crystallinity, ΔH_m is the sample melting enthalpy, $\Delta H_m{}^0$ is the melting enthalpy of 100% crystalline PBAT, and WPBAT is the mass fraction of the PBAT in the blend. The ΔHm^0 value used for the PBAT was 114 $J.g^{-1}$ (Xiao et al., 2009).

2.5.3. X-ray diffraction (XRD) analysis

The crystallinity of polymer composite strongly influences its chemical and mechanical properties. Moreover, the addition of fillers, such as CNC, depending on the filler concentration, can potentially alter the crystallinity of the polymer matrix, acting as nucleating agents (Gan et al., 2020). The crystalline nature of the PBAT/PLA blend and its bionanocomposite film samples were analyzed using a Siemens - D5000 diffractometer operated at 40 kV and 40 mA, with CuKα radiation (λ= 15.4 Å).

2.5.4. Water contact angle measurements

The absorption of water by the surface of the material is linked to the wettability process of the water on the material surface and, consequently, the hydrophilic/hydrophobic character of the material surface. A high degree of wettability between water and material means a greater contact area between them and a greater probability of absorption and more hydrophilic material. Wettability is commonly assessed by the contact angle of the liquid with the solid surface. In this phenomenon, the greater the contact angle, the lower the wettability, that is, the material has a hydrophobic character when the liquid wets less the solid surface in contact. The surface wettability of bionanocomposite films was determined through water contact angle (WCA) measurements using a KSV Theta standard goniometer equipped with a camera to capture the images of water droplets and then determine the contact angles. Deionized water was used to evaluate the wettability properties of these films. Angle measurements were performed in triplicate, and their average values were taken.

2.5.5. Water absorbency test

Water absorbency measurements of the bionanocomposite film samples were performed in triplicate, and the average values were reported. The water absorbency of the bionanocomposite films was evaluated in terms of swelling. Each film sample was sectioned into a 2×2 cm^2 piece, dried at 45 ± 2 °C for 24 hours in a circulating air oven, and preweighed. The preweighed samples were immersed in a petri dish filled with 20 mL of deionized water and remained undisturbed for 24 hours at room temperature until an equilibrium swelling was reached. The samples were removed from deionized water, quickly wiped with filter paper to remove droplets on the surface, and then weighed. The samples were weighed at specific intervals of time until the equilibrium swelling was reached. The swelling ratio was calculated using the following expression, Eq. (3) (Yadav & Chiu, 2019):

$$\text{Swelling Ratio}(\%) = ((W_s\text{-}W_d)/(W_d) \times 100) \tag{3}$$

Where W_s = weight of the swollen samples, W_d = weight of the dry samples in all three replicates.

Table 2
Crystallinity index of SBF and CNC samples.

Samples	I_{002}	I_{AR}	I_C (%)
Sugarcane Bagasse Fiber (SBF)	351	185	47.2
Cellulose Nanocrystals (CNCs)	3429	1030	70.1

2.5.6. Field emission scanning electron microscopy (FESEM) analysis

The surface morphologies of the cryofractured bionanocomposite samples under liquid nitrogen were analyzed by scanning electron microscopy (SEM) using a JEOL-JSM-6701F, microscope accelerating voltage of 1-30 kV, using EDS Thermo-Scientific mod. Noran System Six software, in carbon, sputtered samples.

2.5.7. Mechanical tests

Tensile tests were determined using an INSTRON Testing Machine model 5564, according to ASTM D 882-91, to evaluate the mechanical behavior of the bionanocomposite film samples. Each value obtained represented the average of five samples.

3. Results and discussion

3.1. Cellulose nanocrystal characterization

3.1.1. X-ray diffraction (XRD) analysis

The crystalline structure and the crystallinity index of sugarcane bagasse fiber and cellulose nanocrystal were determined by XRD analysis. XRD patterns were collected from 5° to 90° (2θ). The SBF and cellulose nanocrystal (CNC) exhibited characteristic crystalline peak related to the crystalline structure of cellulose I at around 2θ = 22.5°, which corresponded to the lattice plane (002), and one broad peak at 2θ = 16.5°, corresponded to the lattice plane (110) related to the amorphous domains of cellulose. The crystallinity index (Ic) of SBF and CNC calculated from Eq. (1) is presented in Table 2. The Ic of the SBF and CNC were around 47% and 70%, respectively. These results indicate a predominance of crystalline.

3.1.2. Thermogravimetric analysis (TGA)

According to the obtained TGA and DTG curves of SBF and CNC, two main stage degradations were observed during the thermal analysis of the SBF. The first stage degradation, which occurred at 30–142 ℃, presented a slight weight loss (WL) of about 2% and was attributable to the evaporation of residual water present in the material. The second degradation, which exhibited the higher WL of about 62%, occurred at 230–400 ℃ and referred to the process of thermal decomposition of cellulose, including dehydration, decomposition, and depolymerization of the glycoside units (Yadav & Chiu, 2019). The slow and gradual decreased in WL of about 7.8% observed from 400 to 770 ℃ was

Table 3
Onset temperature (T_{onset}), maximum temperature (T_{max}), and residual weight (RW) obtained from TGA analysis.

Samples	T_{onset} (°C)	T_{max} (°C)	RW (770 °C) (%)
Sugarcane Bagasse Fiber (SBF)	276	330	28.2
Cellulose Nanocrystals (CNCs)	230	270	23.6

assigned to the decomposition of lignin, whereas that of lignin had a broader degradation temperature range between 220 and 600 °C (Jiang, Lawrence, Hussain, Ansell, & Walker, 2019). The onset temperature (T_{onset}) is defined as the temperature at which the WL of the sample becomes apparent, while the maximum temperature (T_{max}) is the maximum thermal degradation temperature, which is the peak of the derivative TGA curve (Herrera et al. 2018). The T_{onset} and T_{max} of SBF were at around 276 °C and 330 °C, respectively. The measured value of residual weight (RW) at 770 °C was at around 28.2%. The degradation process of CNC occurred in three main stages. The first degradation with a slight WL of about 2.7% occurred at 30–144 °C and was attributable to the evaporation of residual water present in the material.

The second stage degradation, which exhibited a higher WL of about 53.4%, started at around 185 °C and ended at approximately 336 °C. In this stage, hydroxyl groups were replaced by acid sulfate groups in the acid hydrolysis step, decreasing the activation energy for the cellulose degradation. The sample becomes less resistant to pyrolysis, with dehydration reactions taking place, releasing water, and catalyzing its decomposition. The third stage, from 336 to 770 °C, presented a gradual WL at around 20.2% as a function of temperature and was associated with cellulose pyrolysis that occurs in the 300 to 600 °C range, and was attributed to the breakdowns of the internal cellulose molecules, which did not make contact with sulfuric acid in acid hydrolysis, for the oxidation and breakdown of charred residues to form gaseous products of low molecular weight. The CNC showed a T_{onset} around 230 °C and T_{max} at approximately 270 °C. The RW at 770 °C was around 23.6% and lower than those of SBF. A similar trend was reported in the literature and was related to the insertion of sulfate groups on the surface of CNC during hydrolysis with sulfuric acid (El Achaby et al., 2017; Roman & Winter, 2004; Sahlin et al. 2018). The onset temperature (T_{onset}), the maximum temperature (T_{max}), and the RW obtained for SBC and CNC are summarized in Table 3. Although the thermal stability of CNC was lower than SBF, it remained high enough for most practical applications. Moreover, the thermal stability of the CNC makes it suitable for the development of sustainable food packaging material based on the PBAT/PLA blend, as proposed in this work, since both the temperature of the processing and the work of these packaging materials are less than the degradation temperature of CNC.

3.1.3. Transmission electron microscopy (TEM) analysis

The TEM image of the cellulose nanocrystals (CNCs) in aqueous suspension of 0.03 g/mL concentration is in Fig. 2a and 2b. The images show the efficiency of acid hydrolysis treatment to obtain cellulose nanocrystals from sugarcane bagasse fiber. The TEM image confirmed the presence of nanocrystals in the suspensions, which consists mainly of individual fibrils of elongated length and diameter in the order of magnitude of nanometers, with needle-like in shape, and with size in the range of 50−150 nm (length) and 1−10 nm (diameter) with a relatively high aspect ratio.

3.2. Blend and bionanocomposite films characterization

3.2.1. Thermogravimetric analysis (TGA)

The TGA curves and derivative thermogram (DTG) curves of PBAT/PLA blend and its bionanocomposite films were obtained. Based on the DTG, two-step degradations were observed for the PBAT/PLA blend and its bionanocomposite films. Similar findings were reported by Shrivastava, Wooi, Hassan, & Inuwa (2018). Furthermore, TGA/DTG results presented a significant difference in residue weight and onset temperature (T_{onset}) of the neat blend compared to bionanocomposite films, as shown in Table 4. The thermal stability of the bionanocomposite films increased with the increased CNC content, which can be corroborated from the lower residue weight value of PBAT/PLA blend film compared to those of bionanocomposite films and with the T_{onset}, T_{max}, and T_{final} values presented in Table 4. Considering that improvement in thermal stability is usually related to an increase in T_{onset} and T_{max}, the film content of 2 wt. % CNC (PBAT/PLA/CNC 2) exhibited optimum thermal stability with more than 25 °C of enhancement in T_{onset}.

As observed from Table 4, the T_{max} of this film increased from 395 to 400 °C, and the T_{final} from 406 to 415 °C. The improvement in thermal stability can be attributed to the CNC particles, which were diffused homogeneously into the matrix and firmly combined, despite the presence of some CNC aggregates, as can be seen in FESEM images (Fig. 4). The collected data clearly indicate that the thermal stability of

Table 4
Thermogravimetric (TGA) and differential scanning calorimetry (DSC) analysis results of PBAT/PLA blend and its bionanocomposite films.

Samples	T_{onset} (°C)	T_{max} (°C)	T_{final} (°C)	RW (%)	T_m (°C)	ΔH_m (Jg^{-1})	Xc (%)
PBAT/PLA Blend	341	395	406	2.6	154.8	4.5	13.2
PBAT/PLA/CNC 1[a]	347	399	410	6.4	154.3	7.6	21.7
PBAT/PLA/CNC 2[b]	368	400	415	4.5	154.9	9.5	26.5

[a] PBAT/PLA content of 1 wt. % of CNC.
[b] PBAT/PLA content of 2 wt. % of CNC.

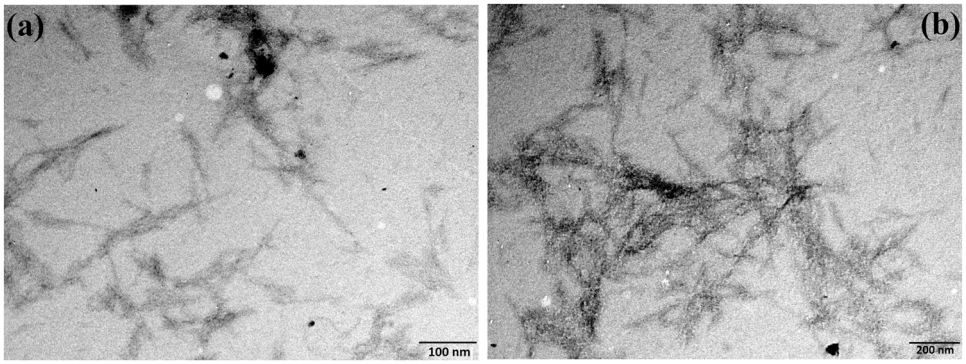

Fig. 2. TEM image of CNC (a) at magnification of 6500 X and (b) 13000 X, respectively.

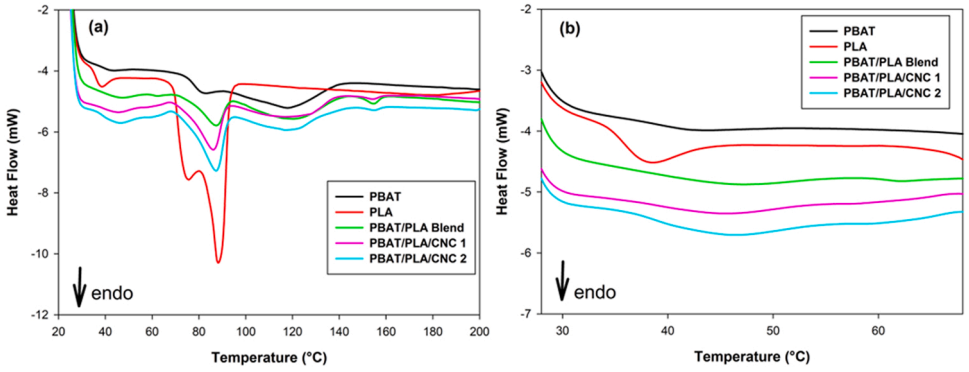

Fig. 3. DSC results, (a) non-isothermal DSC curves for PBAT, PLA and for the PBAT/PLA and PBAT/PLA/CNC blends and (b) glass transition temperatures (Tg).

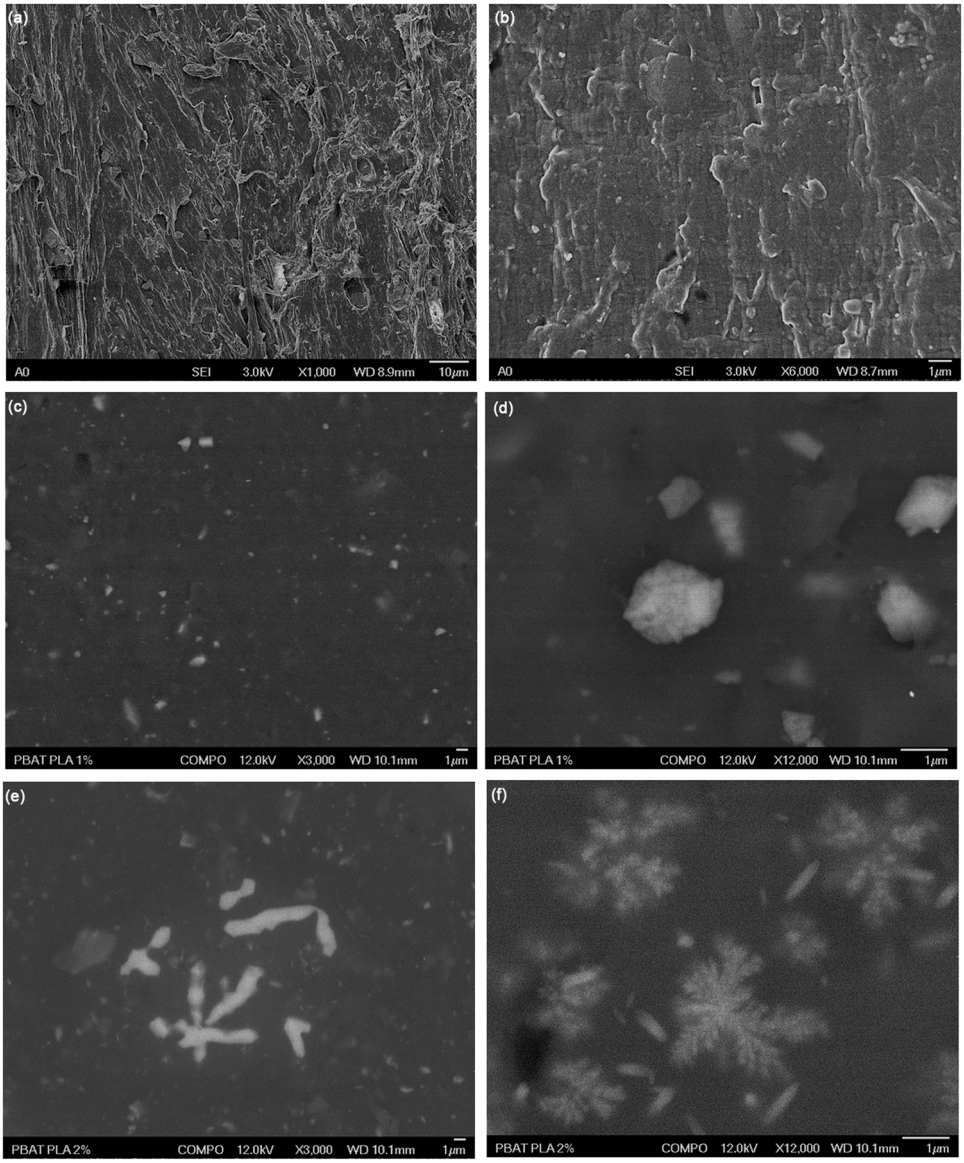

Fig. 4. FESEM images of the PBAT/PLA Blend: (a)1.000 X, (b) 6.000 X; PBAT/PLA/CNC1: (c) 3.000 X, (d)12.000 X; PBAT/PLA/CNC2: (e)3.000 X, (f)12.000 X.

bionanocomposite films was strongly influenced by the intermolecular bonding between the CNC and the PBAT/PLA blend matrix since the bond dissociation energy needed for chain cleavage of the polymer could be enhanced by strong intermolecular bonding. Similar trends were recently reported by Gan et al. (2020). Mandal & Chakrabarty (2014) found that the incorporation of nanocrystalline cellulose (NCC) from sugarcane bagasse in PVOH significantly improved the thermal stability of NCC–PVOH nanocomposites by enhancing the NCC-matrix

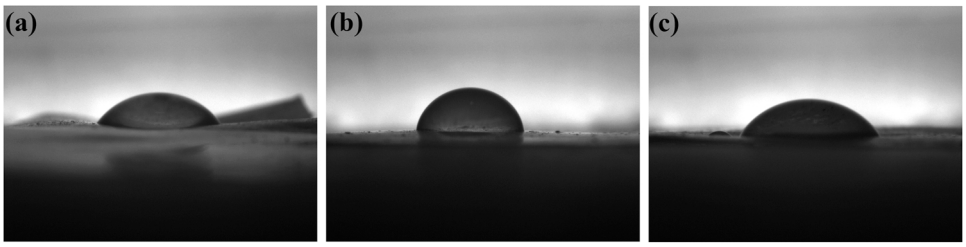

Fig. 5. Image of the water droplet on the surfaces of bionanocomposite films for the contact angles measured: (a) PBAT/PLA Blend; (b) PBAT/PLA/CNC1; (c) PBAT/PLA/CNC2.

interaction through hydrogen bonding. Hai et al. (2020) observed improved thermal stability of chitin nanofiber (CTNF) and bamboo cellulose nanofiber (BACNF) nanocomposites when investigating the thermal degradation of a green nanocomposite. Mondragon, Peña-Rodriguez, González, Eceiza, & Arbelaiz (2015) also reported a significant increase in the thermal stability of a bionanocomposite based on the incorporation of nanocrystalline cellulose (NCC) in the gelatin matrix.

3.2.2. Differential scanning calorimetry (DSC) analysis

Fig. 3(a) shows the non-isothermal DSC curves for PBAT and PLA as well as the PBAT/PLA and PBAT/PLA/CNC blends, and Fig. 3(b) presents the glass transition temperatures (Tg). For PLA, its Tg can be seen in the temperature range between 34 and 43 °C. Then a complex endothermic peak is observed, which refers to the melting of PLA, with peak temperature at 88 °C. PBAT exhibits an endothermic peak with low intensity, referring to its fusion, with peak temperature at 118 °C. In the PBAT/PLA blends, the Tg can not be identified in Fig. 3(b), suggesting that the addition of PBAT in PLA shifted the Tg of PLA to lower temperatures below the range used in the analysis, since PBAT Tg occurs around -33 °C to -39 °C (Kilic, Can, Kodal, & Ozkoc, 2019; Nayak 2010). With the addition of CNC, the Tg of PLA shifts to higher temperatures between 37 °C and 46 °C, indicating the immiscibility of the blends and that the nanocrystals made it difficult to move the amorphous phase, requiring more energy for the event to occur.

Arrieta et al. (2014) reported similar results for poly(lactic acid)/poly(hydroxybutyrate)/cellulose nanocrystals (PLA/PHB/CNCs) blends. The incorporation of PHB in PLA shifted its Tg to lower temperatures from 58.8 °C to 53.5 °C, and the addition of CNCs in the PLA/PHB blend shifted the Tg of PLA to higher temperatures (62.5 °C).

The melting temperature and enthalpy as well as the crystallinity degree of the PBAT/PLA blend and its bionanocomposite films are presented in Table 4. Table 4 indicates that compared to blend, the endothermic melting enthalpy and crystallinity degree of bionanocomposite films increased with the amount of CNC added, but the melting temperature was not changed. The increases in the melting enthalpy and crystallinity degree can be attributed to the high crystallinity degree of CNC.

Table 5
Contact angle degree and swelling ratio of the PBAT/PLA blend film and its bionanocomposite films.

Samples	Contact angle (degree)	Swelling ratio (%)	water absorbency reduction (%)
PBAT/PLA Blend	50.5±1.3	8.6±0.5	-
PBAT/PLA/CNC 1[a]	71.0±1.0	3.9±0.3	- 55
PBAT/PLA/CNC 2[b]	54.0±0.3	2.5±0.2	- 70

[a] PBAT/PLA content of 1 wt.% of CNC.
[b] PBAT/PLA content of 2 wt.% of CNC

3.2.3. Field emission scanning electron microscopy (FESEM) analysis

Fig. 4 is FESEM images of cryofractured surfaces of the bionanocomposite films. Fig. 4a and 4b present an overview of PBAT/PLA blend with magnifications of 1.000× and 6.000×, respectively, illustrating the characteristic morphology of immiscible blends with low adhesion and uniform dispersion of PLA, which is the dispersed phase on the slightly rough surface of the PBAT matrix. The FESEM image of the surface of PBAT/PLA films containing CNCs reveal a smooth surface structure with a homogeneous distribution of CNCs and well-defined occurrence of some aggregated particles on the surface of films, but without any visible cracks or holes, as shown in Fig. 4c and 4d of PBAT/PLA/CNC1 with magnifications of 3.000× and 12.000× and Fig. 4e and 4f of PBAT/PLA/CNC2 with magnifications of 3.000× and 12.000×, respectively. The aggregation of CNCs increased with increasing CNCs content. This effect was mainly due to the existence of strong interactions between the surface of hydroxyl groups of the CNC at the higher loading level as well as the attractive van der Waals forces (George & Sabapathi, 2015; Klemm et al., 2018; Lee et al. 2019; Tayeb, Amini, Ghasemi, & Tajvidi, 2018). Both the strong interactions between the hydroxyl groups of the CNCs and the van der Waals forces contributed to the increased concentration of CNCs, which led to a rapid collision between the CNCs particles during the dispersion process in the PBAT/PLA matrix.

In this case, the CNC-CNC interaction became dominant over the CNC–matrix interaction, which induced the CNC particles to stick together and form aggregates, and the contact area between CNCs and PBAT/PLA matrix was reduced. Its homogeneous dispersion in the matrix was restricted. Such occurrence has been observed in previous studies (Azizi et al. 2014; Chakrabarty & Teramoto, 2018; Dufresne, 2018; El Miri et al., 2016; Klemm et al., 2018; Risyon et al., 2020).

Unlike what the aggregated CNCs presented on the surface of the PBAT/PLA/CNC1 film, Figs. 4c and 4d, the surface of the PBAT/PLA/CNC2 film, Fig. 4e and 4f, displays aggregations of needle-shaped CNCs with lengths up to several microns. Despite the presence of aggregated CNCs, Fig. 4 suggests good adhesion between CNCs and PBAT/PLA blend matrix, which plays an essential role in improving the mechanical performance of the resulting bionanocomposite films.

3.2.4. X-ray diffraction (XRD) analysis

The X-Ray diffraction patterns of PBAT/PLA blend and bionanocomposite films had peaks at around $2\theta = 9.6°$, 17.6°, 18.8°, 26.7°, 28.6°, and 29.6°, attributed mainly to PBAT, and abroad, amorphous halo in the range of 16° to 24.8°, which might be the contribution of PLA. According to literature, the characteristic diffractogram of neat PLA displays a broad, amorphous halo, indicating its amorphous state, with the prominent peaks at $2\theta = 16.6°$ and 19.1°, and two smaller peaks at $2\theta = 14.7°$ and 22.3° (Papadopoulou et al., 2019). The diffractograms of the bionanocomposite films revealed significant increases in the intensity of crystalline peaks, which were approximately $2\theta = 9.6°$, 18.8°, 28.6°, and 29.6°, with the increased amount of CNC content. On the other hand, the characteristic crystalline peak related to CNC was not visible in all bionanocomposite films. This can presumably be ascribed to good interactions between the PBAT/PLA blend and CNC, which

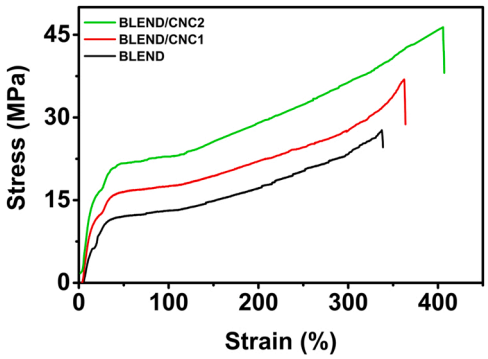

Fig. 6. Stress-Strain curves for PBAT/PLA blend and its bionanocomposite films.

contributed to an increase of crystallinity degree observed in the DSC results, and consequently to improved thermal stability and mechanical properties of bionanocomposite films when compared to PBAT/PLA blend film.

3.2.5. Water contact angle measurements

The water droplet image on the bionanocomposite film surfaces and the contact angle (WCA) measured for different cellulose nanocrystal content from 0 to 2 wt.% are shown in Fig. 5 and Table 5, respectively.

The WCA of the bionanocomposite film surface was measured to evaluate the hydrophilic/hydrophobic character of the film. The water contact angle of bionanocomposite films increased with increased CNC content from 0 to 2 wt. % (Fig. 5). The neat PBAT/PLA blend film presented a lower contact angle value of 50°, as expected due to the low hydrophobic character of PBAT. The addition of 1 wt. % of CNCs increased the contact angle from 50 to 71°. However, when the CNC content was 2 wt. %, the contact angle increased only 54° (Table 5). The surface hydrophobicity of CNCs and their dispersion in the blend film may explain these results. The surface hydrophobicity of CNC is better than that of the blend, which probably reduces diffusion of water molecules in the matrix. On the other hand, when the CNC content was increased to 2 wt. %, some CNC were not completely blended with PBAT/PLA matrix as shown at FESEM images (Fig. 4(c–f)), and aggregated CNC appeared on the surface of the bionanocomposite films. The amount of aggregated CNC drastically increased on the bionanocomposite surface with content of 2 wt. % of CNC. Whereas at 1 wt. % of CNCs, the more homogenous dispersion on the blend surface and higher contact angle may suggest that the increase of aggregated CNC decreased the contact angles of the bionanocomposite film. Similar findings have previously been reported (Goudarzi, Shahabi-Ghahfarrokhi, & Babaei-Ghazvini, 2017; Hai et al., 2020; Yadav & Chiu, 2019).

3.2.6. Water absorbency test

The swelling ratio for water absorbency measurements of the bionanocomposite films is presented in Table 5.

As CNC content increased from 0% to 2%, the swelling ratio decreased from 8.6 to 2.5%. This indicates that the bionanocomposite films containing 1 and 2 wt.% of CNC exhibited about 55% and about 70% less water absorbency properties than the PBAT/PLA blend film, respectively. Thus, incorporation of CNCs increased the hydrophobicity of the films, which is essential for food packaging applications due to the greater crystallinity of the CNCs than PBAT/PLA blend, which, upon incorporation, acts as a barrier hindering PBAT/PLA blend molecules from swelling and thereby lessening the water absorbency. Furthermore, as the CNCs are crystalline particles, they could inhibit the water diffusion through the PBAT/PLA blend. This result is consistent with other studies (Fortunati et al., 2014; Wang et al., 2016; Wu, Farnood, O'Kelly, & Chen, 2014; Yadav & Chiu, 2019).

Table 6
Mechanical properties of the PBAT/PLA blend film and its bionanocomposite films.

Bionanocomposite films	Thickness (μm)	Tensile strength at break (MPa)	Elongation at break (%)	Young's modulus (MPa)
PBAT/PLA Blend[a]	60 ± 1.0	29.6 ± 1.6	370 ± 27	136 ± 10
PBAT/PLA/CNC 1[b]	64 ± 1.3	37.3 ± 2.5	460 ± 32	220 ± 12
PBAT/PLA/CNC 2[c]	63 ± 1.2	44.7 ± 2.3	478 ± 39	296 ± 17

[a] PBAT/PLA blend.
[b] PBAT/PLA content of 1 wt.% of CNC.
[c] PBAT/PLA content of 2 wt.% of CNC.

Table 7
Mechanical properties of commercial plastic-based films.

Commercial plastic-based films	Tensile strength (MPa)	Elongation at break (%)	Young's modulus (MPa)
Low-density polyethylene (LDPE)	7.00 – 34.5	50.0 – 1000	140 – 480
Linear low-density polyethylene (LLDPE)	10.0 – 37.3	0.80 – 1000	110 – 413
High-density polyethylene (HDPE)	23.0 – 40.0	400 – 1700	200 – 1350
Poly(vinyl chloride (PVC)	42.0 – 55.0	20.0 – 180	5.52 – 3230
Poly(propylene (PP)	27.0 – 98.0	200 – 1000	700 – 7510
Polyamide 66 (PA66)	31.0 – 45.0	40.0 – 170	400 – 3310
Poly(ethylene terephthalate (PET)	2.10 – 90.0	4.00 – 600	107 – 3500

[a] based on data presented by MatWeb("Online Materials Information Resource - MatWeb," 2002) and Otoni et al. (2017)

3.2.7. Mechanical tests

Typical stress-strain curves of PBAT/PLA blend and its bionanocomposite films are in Fig. 6. These curves are based on average values calculated from the data obtained for five test specimens. Fig. 6 indicates that all film samples presented a mechanical behavior representative of ductile materials with a characteristic yield point, large plastic deformation, and high elongation values at break. A remarkable increase in tensile strength at break, Young modulus, and elongation at break of neat PBAT/PLA blend film due to the addition of CNCs were observed, contrary to the expected inverse relationship between tensile strength and elongation at break (Table 6).

Similar mechanical behaviors were reported by Reddy & Rhim (2014), for crystalline nanocellulose incorporated into agar, and by Mandal & Chakrabarty (2014), in their study of the incorporation of nanocellulose from sugarcane bagasse into poly(vinyl alcohol).

In the present experiment, the tensile strength, elongation at break, and Young's modulus of the PBAT/PLA film content of 1 wt. % of CNCs increased by around 27%, 24%, and 62%, respectively, compared to PBAT/PLA blend film. The tensile strength, elongation at break, and Young's modulus were increased by around 52%, 29%, and 118%, respectively, by increasing CNC content from 1 wt. % to 2 wt. %. This behavior may be attributed to the inherent chain stiffness and rigidity of CNC (elastic modulus from 130 to 250 GPa) (Reddy & Rhim, 2014), the high aspect ratio (1–10 nm in diameter and 50–150 nm in length), and the strong interfacial interaction induced through hydrogen bonding between the CNC and the PBAT/PLA blend matrix. The improvement in the mechanical performance of the blend film containing 2 wt. % CNCs suggests that the increase of the amount of CNC aggregates on the surface of the film, as can be noted in the FESEM image (Fig. 4e and 4f), was not large enough to lead to non-uniform stress distribution in the films. This was able to reduce the interaction between the CNCs and PBAT/-PLA blend matrix, and consequently reduce the mechanical behavior of the film.

The increases in percent elongation at break, which measures flexibility or ductility of films, in tensile strength and Young's modulus, make these bionanocomposite films strong and tough, the main

Fig. 7. Visual appearance of bionanocomposite films: (a) PBAT/PLA Blend, (b) PBAT/PLA/CNC1, and (c) PBAT/PLA/CNC2.

mechanical characteristic required for food packaging applications. Furthermore, the mechanical test values of the bionanocomposite films are comparable to those of some commercial plastic-based films used in food packaging, as can be seen in Tables 6 and 7, which was based on data presented by MatWeb (2002) and Otoni et al. (2017). However, Young's modulus of the films was smaller than those of the polypropylene (PP) and polyamide 66 (PA66) film grades (Table 6). In addition, the visual appearance of bionanocomposite films exhibited transparency and no visual aggregates, which are important features for use in food packaging (Fig. 7). The order of visual transparency of films is as follows:

PBAT/PLA Blend > PBAT/PLA/CNC1 > PBAT/PLA/CNC2

4. Conclusions

In the present work, CNCs consisting of individual fibrils of elongated length and diameter in nanometers were obtain. The thermal stability of CNCs was lower than SBF but remained suitable for developing sustainable food packaging materials, whose processing and work temperatures are less than the degradation temperature of CNC. Bionanocomposite films presented a significant improvement in the hydrophobic character and thermal stability compared to blend. Their evaluated mechanical values were comparable to those of some commercial plastic-based films used in food packaging. In conclusion, the proposed bionanocomposite films represent an interesting alternative to produce sustainable food packaging materials.

Funding sources

The authors appreciate the funding from FAPESP/ Process Number 2019/00862-9, and IAEA-CRP No. 17760/RO.

Authorship contribution statement

Marcio S. Andrade: Conceptualization, Investigation, Data curation. **Otávio H.** Conceptualization, Data curation. **Robson S. Costa:** Investigation, Data curation. **Marcus V.S. Seixas:** Methodology, Formal analysis, Validation. **Rita C.L.B. Rodrigues:** Methodology, Supervision, Writing - review & editing. **Esperidiana A.B. Moura:** Conceptualization, Formal analysis, Supervision, Funding acquisition, Project administration, Writing - review & editing.

Declaration of Competing Interest

The authors declare that they have no known competing financial interests or personal relationships that could have appeared to influence the work reported in this paper.

Acknowledgments

The authors wish to thank FAPESP(Brazil)/Process Number 2019/00862-9, IAEA-CRP(Vienna) No. 17760/RO, and CAPES(Brazil) for the support provided on this work.

Appendix A. Supporting information

Supplementary data associated with this article can be found in the online version at doi:10.1016/j.fpsl.2021.100807.

References

El Achaby, M., El Miri, N., Aboulkas, A., Zahouily, M., Bilal, E., Barakat, A., & Solhy, A. (2017). Processing and properties of eco-friendly bio-nanocomposite films filled with cellulose nanocrystals from sugarcane bagasse. *International Journal of Biological Macromolecules, 96*, 340–352. https://doi.org/10.1016/j.ijbiomac.2016.12.040

Arrieta, M. P., Fortunati, E., Dominici, F., Rayón, E., López, J., & Kenny, J. M. (2014). Multifunctional PLA–PHB/cellulose nanocrystal films: Processing, structural and thermal properties. *Carbohydrate Polymers, 107*, 16–24. https://doi.org/10.1016/j.carbpol.2014.02.044

Azizi, S., Ahmad, M., Bin, Hussein, M. Z., Ibrahim, N. A., & Namvar, F. (2014). Preparation and properties of poly(vinyl alcohol)/chitosan blend bionanocomposites reinforced with cellulose nanocrystals/ZnO-Ag multifunctional nanosized filler. *International Journal of Nanomedicine, 9*, 1909–1917. https://doi.org/10.2147/IJN.S60274

Chakrabarty, A., & Teramoto, Y. (2018). Recent advances in nanocellulose composites with polymers: A guide for choosing partners and how to incorporate them. *Polymers, 10*. https://doi.org/10.3390/polym10050517

Coles, R., Kirwan, M.J., 2003. Edited by. Blackwell Publishing Ltd Editorial, Boca Raton, FL-USA.

Dufresne, A. (2018). Cellulose nanomaterials as green nanoreinforcements for polymer nanocomposites. *Philosophical Transactions of the Royal Society A: Mathematical, Physical and Engineering Sciences, 376*. https://doi.org/10.1098/rsta.2017.0040

El Fawal, G., Hong, H., Song, X., Wu, J., Sun, M., Zhang, L., … Wang, H. (2020). Polyvinyl alcohol/hydroxyethylcellulose containing ethosomes as a Scaffold for transdermal drug delivery applications. *Applied Biochemistry and Biotechnology, 191*, 1624–1637. https://doi.org/10.1007/s12010-020-03282-1

Fortunati, E., Luzi, F., Puglia, D., Dominici, F., Santulli, C., Kenny, J. M., & Torre, L. (2014). Investigation of thermo-mechanical, chemical and degradative properties of PLA-limonene films reinforced with cellulose nanocrystals extracted from Phormium tenax leaves. *European Polymer Journal, 56*, 77–91. https://doi.org/10.1016/j.eurpolymj.2014.03.030

Gan, I., & Chow, W. S. (2018). Antimicrobial poly(lactic acid)/cellulose bionanocomposite for food packaging application: A review. Food Packag. *Shelf Life, 17*, 150–161. https://doi.org/10.1016/j.fpsl.2018.06.012

Gan, P. G., Sam, S. T., Abdullah, M. F., & bin, Omar, M. F. (2020). Thermal properties of nanocellulose-reinforced composites: A review. *Journal of Applied Polymer, 137*. https://doi.org/10.1002/app.48544

George, J., & Sabapathi, S. N. (2015). Cellulose nanocrystals: Synthesis, functional properties, and applications. *Nanotechnology, Science and Applications, 8*, 45–54. https://doi.org/10.2147/NSA.S64386

Goudarzi, V., Shahabi-Ghahfarrokhi, I., & Babaei-Ghazvini, A. (2017). Preparation of ecofriendly UV-protective food packaging material by starch/TiO2 bio-nanocomposite: Characterization. *International Journal of Biological Macromolecules, 95*, 306–313. https://doi.org/10.1016/j.ijbiomac.2016.11.065

Hai, L. V., Choi, E. S., Zhai, L., Panicker, P. S., & Kim, J. (2020). Green nanocomposite made with chitin and bamboo nanofibers and its mechanical, thermal and biodegradable properties for food packaging. *International Journal of Biological Macromolecules, 144*, 491–499. https://doi.org/10.1016/j.ijbiomac.2019.12.124

Herrera, M., Thitiwutthisakul, K., Yang, X., Rujitanaroj, P. on, Rojas, R., & Berglund, L. (2018). Preparation and evaluation of high-lignin content cellulose nanofibrils from eucalyptus pulp. *Cellulose, 25*, 3121–3133. https://doi.org/10.1007/s10570-018-1764-9

Jamróz, E., Kulawik, P., & Kopel, P. (2019). The effect of nanofillers on the functional properties of biopolymer-based films: A review. *Polymers, 11*, 1–43. https://doi.org/10.3390/polym11040675

Jiang, Y., Lawrence, M., Hussain, A., Ansell, M., & Walker, P. (2019). Comparative moisture and heat sorption properties of fibre and shiv derived from hemp and flax. *Cellulose, 26*, 823–843. https://doi.org/10.1007/s10570-018-2145-0

Kilic, N. T., Can, B. N., Kodal, M., & Ozkoc, G. (2019). Compatibilization of PLA/PBAT blends by using Epoxy-POSS. *Journal of Applied Polymer Science, 136*(12), 47217. https://doi.org/10.1002/app.47217

Klemm, D., Cranston, E. D., Fischer, D., Gama, M., Kedzior, S. A., Kralisch, D., … Rauchfuß, F. (2018). Nanocellulose as a natural source for groundbreaking applications in materials science: Today's state. *Materials Today, 21*, 720–748. https://doi.org/10.1016/j.mattod.2018.02.001

Kumar, S., Mukherjee, A., & Dutta, J. (2020). Chitosan based nanocomposite films and coatings: Emerging antimicrobial food packaging alternatives. *Trends in Food Science and Technology, 97*, 196–209. https://doi.org/10.1016/j.tifs.2020.01.002

Lee, H. J., Lee, H. S., Seo, J., Kang, Y. H., Kim, W., & Kang, T. H. K. (2019). State-of-the-art of cellulose nanocrystals and optimal method for their dispersion for construction-related applications. *Applied Science, 9*, 1–14. https://doi.org/10.3390/app9030426

Mandal, A., & Chakrabarty, D. (2014). Studies on the mechanical, thermal, morphological and barrier properties of nanocomposites based on poly(vinyl alcohol) and nanocellulose from sugarcane bagasse. *Journal of Industrial and Engineering Chemistry, 20*, 462–473. https://doi.org/10.1016/j.jiec.2013.05.003

Marsh, K., & Bugusu, B. (2007). Food packaging - Roles, materials, and environmental issues: Scientific status summary. *Journal of Food Science, 72*. https://doi.org/10.1111/j.1750-3841.2007.00301.x

El Miri, N., El Achaby, M., Fihri, A., Larzek, M., Zahouily, M., Abdelouahdi, K., & Solhy, A. (2016). Synergistic effect of cellulose nanocrystals/graphene oxide nanosheets as functional hybrid nanofiller for enhancing properties of PVA nanocomposites. *Carbohydrate Polymer, 137*, 239–248. https://doi.org/10.1016/j.carbpol.2015.10.072

Mondragon, G., Peña-Rodriguez, C., González, A., Eceiza, A., & Arbelaiz, A. (2015). Bionanocomposites based on gelatin matrix and nanocellulose. *European Polymer Journal, 62*, 1–9. https://doi.org/10.1016/j.eurpolymj.2014.11.003

Mori, N., 2015. Etanol celulósico a partir da palha e do bagaço de cana-de-açúcar: pré-tratamentos e conversão biotecnológica não convencionais. Teses.Usp.Br.

Moustafa, H., Youssef, A. M., Darwish, N. A., & Abou-Kandil, A. I. (2019). Eco-friendly polymer composites for green packaging: Future vision and challenges. *Composites Part B: Engineering, 172*, 16–25. https://doi.org/10.1016/j.compositesb.2019.05.048

Nayak, S. K. (2010). Biodegradable PBAT/starch nanocomposites. *Polymer-Plastics Technology and Engineering, 49*(14), 1406–1418. https://doi.org/10.1080/03602559.2010.496397

Online Materials Information Resource - MatWeb, 2002.

Otoni, C. G., Avena-Bustillos, R. J., Azeredo, H. M. C., Lorevice, M. V., Moura, M. R., Mattoso, L. H. C., & McHugh, T. H. (2017). Recent advances on edible films based on fruits and vegetables—A review. *Comprehensive Reviews in Food Science and Food Safety, 16*, 1151–1169. https://doi.org/10.1111/1541-4337.12281

Papadopoulou, E. L., Paul, U. C., Tran, T. N., Suarato, G., Ceseracciu, L., Marras, S., … Athanassiou, A. (2019). Sustainable active food packaging from poly(lactic acid) and cocoa bean shells. *ACS Applied Materials & Interfaces, 11*, 31317–31327. https://doi.org/10.1021/acsami.9b09755

Raheem, D. (2013). Application of plastics and paper as food packaging materials - An overview. *Emirates Journal of Food and Agriculture, 25*, 177–188. https://doi.org/10.9755/ejfa.v25i3.11509

Rana, D., Bag, K., Bhattacharyya, S. N., & Mandal, B. M. (2000). Miscibility of poly (styrene-co-butyl acrylate) with poly (ethyl methacrylate): Existence of both UCST and LCST. *Journal of Polymer Science Part B: Polymer Physics, 38*(3), 369–375. https://doi.org/10.1002/(SICI)1099-0488(20000201)38:3<369. AID-POLB3>3.0.CO;2-W.

Rana, D., Mandal, B. M., & Bhattacharyya, S. N. (1993). Miscibility and phase diagrams of poly (phenyl acrylate) and poly (styrene-co-acrylonitrile) blends. *Polymer, 34*(7), 1454–1459. https://doi.org/10.1016/0032-3861(93)90861-4

Rana, D., Mandal, B. M., & Bhattacharyya, S. N. (1996). Analogue calorimetric studies of blends of poly (vinyl ester) s and polyacrylates. *Macromolecules, 29*(5), 1579–1583. https://doi.org/10.1021/ma950954n

Reddy, J. P., & Rhim, J. W. (2014). Characterization of bionanocomposite films prepared with agar and paper-mulberry pulp nanocellulose. *Carbohydrate Polymers, 110*, 480–488. https://doi.org/10.1016/j.carbpol.2014.04.056

Risyon, N. P., Othman, S. H., Basha, R. K., & Talib, R. A. (2020). Characterization of polylactic acid/halloysite nanotubes bionanocomposite films for food packaging. *Food Packaging and Shelf Life, 23*, Article 100450. https://doi.org/10.1016/j.fpsl.2019.100450

Rocca-Smith, J. R., Pasquarelli, R., Lagorce-Tachon, A., Rousseau, J., Fontaine, S., Aguié-Béghin, V., … Karbowiak, T. (2019). Toward sustainable PLA-based multilayer complexes with improved barrier properties. *ACS Sustainable Chemistry & Engineering, 7*, 3759–3771. https://doi.org/10.1021/acssuschemeng.8b04064

Rodrigues, R., de, C. L. B., Rocha, G. J. M., Rodrigues, D., Filho, H. J. I., Felipe, M., … Pessoa, A. (2010). Scale-up of diluted sulfuric acid hydrolysis for producing sugarcane bagasse hemicellulosic hydrolysate (SBHH). *Bioresource Technology, 101*, 1247–1253. https://doi.org/10.1016/j.biortech.2009.09.034

Roman, M., & Winter, W. T. (2004). Effect of sulfate groups from sulfuric acid hydrolysis on the thermal degradation behavior of bacterial cellulose. *Biomacromolecules, 5*, 1671–1677. https://doi.org/10.1021/bm034519+

Sahlin, K., Forsgren, L., Moberg, T., Bernin, D., Rigdahl, M., & Westman, G. (2018). Surface treatment of cellulose nanocrystals (CNC): Effects on dispersion rheology. *Cellulose, 25*, 331–345. https://doi.org/10.1007/s10570-017-1582-5

Shrivastava, N. K., Wooi, O. S., Hassan, A., & Inuwa, I. M. (2018). Mechanical and flammability properties of poly(lactic acid)/poly(butylene adipate-co-terephthalate) blends and nanocomposites: Effects of compatibilizer and graphene. *Malaysian Journal of Fundamental and Applied Sciences, 14*, 425–431. https://doi.org/10.11113/mjfas.v14n4.1233

Tayeb, A. H., Amini, E., Ghasemi, S., & Tajvidi, M. (2018). Cellulose nanomaterials-binding properties and applications: A review. *Molecules, 23*, 1–24. https://doi.org/10.3390/molecules23102684

Vasile, C. (2018). Polymeric nanocomposites and nanocoatings for food packaging: A review. *Materials, 11*. https://doi.org/10.3390/ma11101834

Wang, Q., Hu, J., Shen, F., Mei, Z., Yang, G., Zhang, Y., … Deng, S. (2016). Pretreating wheat straw by the concentrated phosphoric acid plus hydrogen peroxide (PHP): Investigations on pretreatment conditions and structure changes. *Bioresource Technology, 199*. https://doi.org/10.1016/j.biortech.2015.07.112

Wu, T., Farnood, R., O'Kelly, K., & Chen, B. (2014). Mechanical behavior of transparent nanofibrillar cellulose-chitosan nanocomposite films in dry and wet conditions. *Journal of the Mechanical Behavior of Biomedical Materials, 32*, 279–286. https://doi.org/10.1016/j.jmbbm.2014.01.014

Xiao, H., Lu, W., & Yeh, J.-T. (2009). Crystallization behavior of fully biodegradable poly (lactic acid)/poly(butylene adipate- *co* -terephthalate) blends. *Journal of Applied Polymer Science, 112*, 3754–3763. https://doi.org/10.1002/app.29800

Yadav, M., & Chiu, F. C. (2019). Cellulose nanocrystals reinforced κ-carrageenan based UV resistant transparent bionanocomposite films for sustainable packaging applications. *Carbohydrate Polymers, 211*, 181–194. https://doi.org/10.1016/j.carbpol.2019.01.114

Zhong, Y., Godwin, P., Jin, Y., & Xiao, H. (2020). Biodegradable polymers and green-based antimicrobial packaging materials: A mini-review. *Advanced Industrial and Engineering Polymer Research, 3*, 27–35. https://doi.org/10.1016/j.aiepr.2019.11.002